

THE MID-INFRARED VARIABILITY OF QUASARS: TYPICAL VALUES AND EXTREME OUTLIERS

NICHOLAS P. ROSS¹, AARON MEISNER², DANIEL STERN³, DAVID J. SCHLEGEL², ANDREW DRAKE⁴, MATTHEW GRAHAM⁴, ET AL., FOR THE DECALS CONSORTIUM.

(Dated: March 31, 2017)

Draft version March 31, 2017

ABSTRACT

We present the mid-infrared light-curves for 248 quasars that show large, >0.5 mag peak-to-peak, variation in either the WISE W1 or W2 (3.4 or 4.6 μ m) bands. Our motivation is to quantify and understand the ubiquity and processes involved in luminous AGN obscuration. The quasars are part of the SDSS-I/II or SDSS-III: BOSS Quasar surveys, a superset of over 200,000 objects with at least one epoch of spectroscopy. The IR light curves are from the WISE, NEOWISE and NEOWISE-R missions. Critically we employ new DECaLS data, and find objects that were ‘traditional’ blue quasars (and appear so in SDSS imaging) but turn red in color in DECaLS, and are often now seen as extended. In particular, we present the $z = 0.378$ quasar SDSS J110057.70-005304.5 as a quasar that is transitioning from a blue continuum sloped object to become a “Changing-Look” quasar – with the prominence of the H β and H γ broad-emission lines being dramatically reduced. What makes J110057 particularly interesting, however, is (by selection) its associated short-term IR variability, and dramatic reddening in the optical continuum during the transition to its non-broad line state. (**TBD!!**) We explore simple models of quasar obscuration, and given the short observed timescales (≈ 7 years in the rest frame) find it very hard to explain this behaviour.

Subject headings: WISE, QSOs

1. INTRODUCTION

The reprocessing of UV/optical photons by micron sized carbonates and silicates around an AGN central engine leads to the prodigious emission of infrared (IR) emission (see Elitzur (2014) for review on AGN infrared emission; Netzer (2015) for a review on the Unified Model of Active Galactic Nuclei, and Draine (2003) for a review on dust).

With the energy released by the accretion of material onto a galactic central engine black hole being comparable to the energy released in nuclear fusion having a full accounting of the bolometric output from a luminous AGN, i.e. a quasar, is a critical part of any contemporary galaxy and AGN model and evolutionary theory (e.g., Rosas-Guevara et al. 2016; Bower et al. 2017; McAlpine et al. 2017; Pillepich et al. 2017). Thus, identifying AGN in the IR, and in particular at $\sim 10\mu\text{m}$ where the AGN contribution to the SED peaks (REFs) is of key interest. Indeed, many studies have explored the utilization of mid-IR (3-30 μm rest) to identify and characterize AGN and quasars (Lacy et al. 2004; Stern et al. 2005; Martínez-Sansigre et al. 2006; Richards et al. 2009; Donley et al. 2012; Stern et al. 2012; Banerji et al. 2013; Assef et al. 2013; Richards et al. 2015; Timlin et al. 2016).

Along with the raw energy output, of further critical importance to understanding in detail the physical pro-

cesses of the AGN, and the potential for “feedback” on the host galaxy, is the time-dependent nature of the obscuring, dusty material. Although this is thought to be a dusty rotating “torodial” structure on \sim parsec scales, apart from a few very local case studies (e.g. VLT MIR interferometry objects) we are currently very ignorant to the geometry and topology of the AGN IR emitting region.

As such, observing, and characterizing the MIR *light curves* (LCs) of luminous AGN, would garnish major clues into the variable nature of the energy output of the central engine, along with key tests and constraints on the “AGN unified model”.

In this paper, we use the data from the Wide-Field Infrared Survey Explorer (WISE; Wright et al. 2010), and in particular the NEOWISE-R mission (Mainzer et al. 2014; Meisner et al. 2016), combined with the Sloan Digital Sky Survey quasar catalogs (DR7Q Schneider et al. 2010) and Dark Energy Camera Legacy Survey (DECaLS Lang et al. 2016) to identify 105 quasars (from a sample of 105,000) with large changes, $|\Delta \text{ mag}| > 0.5$, in their MIR LCs.

Kozłowski et al. (2010) and use the multi-epoch, mid-infrared Spitzer Deep Wide-Field Survey to investigate the variability of objects in 8.1 deg 2 of the NOAO Deep Wide Field Survey Botes field. These authors perform a difference image analysis of the four available epochs between 2004 and 2008, over 8.1 deg 2 , focusing on the deeper 3.6 and 4.5 m bands. Out of 474,179 analyzed sources, 1.1% meet their standard variability selection criteria that the two light curves are strongly correlated and that their joint variance exceeds that for all sources with the same magnitude by 2σ . Kozłowski et al. (2016) redo this analysis with a longer baseline.

In Section 2 we describe our datasets and methods for finding the MIR variable quasars, including false posi-

npross@roe.ac.uk

¹ Institute for Astronomy, University of Edinburgh, Royal Observatory, Blackford Hill, Edinburgh EH9 3HJ, United Kingdom

² Lawrence Berkeley National Laboratory, 1 Cyclotron Road, Berkeley, CA 94240, U.S.A.

³ Jet Propulsion Laboratory, California Institute of Technology, 4800 Oak Grove Drive, Mail Stop 169-221, Pasadena, CA 91109, USA

⁴ California Institute of Technology, 1200 East California Boulevard, Pasadena, CA 91125, USA

tive checks. In Section 3 we present our sample and the place the Extreme-IR Changers in context of the general QSO population. In Section 4 we *potentially* say “something” about obscuration rates and draw our conclusions. The (online) Appendix gives the full details of our sample. Because of established conventions, we report SDSS magnitudes on the AB zero-point system (Oke & Gunn 1983; Fukugita et al. 1996), while the WISE magnitudes are calibrated on the Vega system (Wright et al. 2010).

2. DATA

We utilize three large datasets for our investigations: the 5-band, optical Sloan Digital Sky Survey (SDSS; all the usual refs), the 3-band optical Dark Energy Camera Legacy Survey (Lang et al. 2016, DECaLS), and data from the WISE mission. Crucially, data from all three surveys is combined, details of which can be found at legacysurvey.org. We summarize the salient details here.

2.1. Optical Data

2.1.1. SDSS and SDSS-III: BOSS

The SDSS is described in full detail elsewhere (Fukugita et al. 1996; Gunn et al. 1998; York et al. 2000; Hogg et al. 2001; Lupton et al. 2001; Stoughton et al. 2002; Smith et al. 2002; Pier et al. 2003; Ivezić et al. 2004; Gunn et al. 2006; Tucker et al. 2006; Padmanabhan et al. 2008). The third incarnation of the SDSS, SDSS-III is described in Eisenstein et al. (2011) with the Baryon Oscillation Spectroscopic Survey (BOSS) being detailed in Dawson et al. (2013). The final data release paper from SDSS-III was the Data Release 12 (Alam et al. 2015).

We use the SDSS Seventh Data Release Quasar Catalog (DR7Q; Schneider et al. 2010; Shen et al. 2011) and the SDSS-III Twelve Data Release (DR12Q; Páris et al. 2017). SDSS quasar targets with $i \leq 19.1$ were selected if the colors were consistent with being at redshift $z \lesssim 3$, and $i \leq 20.2$ objects were selected if $z \gtrsim 3$, as outlined in Richards et al. (2002). BOSS quasar targets are selected to a magnitude limit of $g \leq 22.0$ or $r \leq 21.85$, with the primary goal to select quasars in the redshift range $2.2 \leq z \leq 3.5$ as described by Ross et al. (2012, and references therein). In both SDSS and BOSS, quasar targets are also selected if they are matched within $2''$ ($1''$ in the case of BOSS) of an object in the Faint Images of the Radio Sky at Twenty-cm (FIRST) catalog of radio sources (Becker et al. 1995). Both the SDSS DR7Q and BOSS DR12Q include quasars that were selected by algorithms other than the main quasar selections; these sources appear in the catalog due to being targeted by the respective galaxy selections, being a ‘serendipitous’ (Stoughton et al. 2002) or ‘special’ (Adelman-McCarthy et al. 2006) target in SDSS, or an ‘ancillary’ target in BOSS (Dawson et al. 2013; Alam et al. 2015; SDSS Collaboration et al. 2016).

2.1.2. DECaLS: Dark Energy Camera Legacy Survey

The Dark Energy Camera Legacy Survey (DECaLS; Lang et al. 2016) is taking deep 3-band g, r, z imaging over 10,000deg of the Northern Sky that is accessible from the Cerro Tololo International Observatory site. As of writing the DECaLS is ongoing.

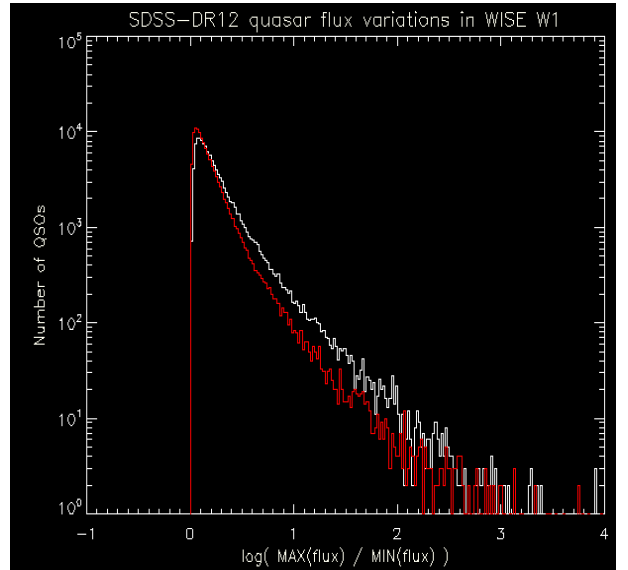


FIG. 1.— The distribution of the maxima and minima flux in $W1$ for the $\sim 240k$ high-confidence quasars in the SDSS-III: BOSS DR12. The red distribution is if one replaces fluxes with a mean flux+measurement error for each observation. Note, since the log is being plotted, the difference between the two lines shows a significant variable population. There are ~ 1000 quasars where the $W1$ flux varies by more than a factor of 2 with a > 5 sigma confidence. Some have a poor χ^2 fits.

2.2. Infrared Data

As noted in Mainzer et al. (2014) and Meisner et al. (2016), after its initial launch, cryogenic mission, and a period of hibernation, the WISE satellite was reactivated, and recommenced surveying the sky in its two shorter wavebands, $W1$ and $W2$. This $W1/W2$ survey is referred to as NEOWISE-Reactivation or NEOWISER.

We directly use the data from Meisner et al. (2016) which employs an adaptation of the unWISE Lang (2014) image coaddition framework.

From the Tractor catalog column descriptions, you will see that DR3 includes sparse WISE $W1/W2$ light curves for every optically detected source (WISE_LC*). These WISE light-curves are measured by forced-photometry of time-resolved unWISE coadds. Currently, in the DECaLS footprint, there are typically four epochs, sometimes five, and very rarely only three. These light curves typically span a $\sim 4\text{-}5$ year time baseline, $\sim 2010\text{-}2014$.

The distribution of the maxima and minima flux in $W1$ for the $\sim 240k$ high-confidence quasars in the SDSS-III: BOSS DR12 is given in Figure 1.

2.3. “False Positive Checks”

Figure 2 is the distribution of $(\max-\min)/\text{error}$ in the MIR fluxes. (Should also be looking at the SDSS stars as a control sample (don't have those on my laptop). The WISE magnitude range for those stars will be quite different, though, since they have the same optical magnitude range but are fainter in WISE.)

$W1$ and $W2$ lightcurves for $\sim 200,000$ SDSS spectroscopic quasars were extracted from Data Release 3 (DR3) of the Dark Energy Camera Legacy Survey (DECaLS). These light curves span from the beginning of the WISE mission (2010 January) through the first-year of NEOWISER operations (2014 December). In detail, the $W1/W2$ light curves are obtained by performing forced

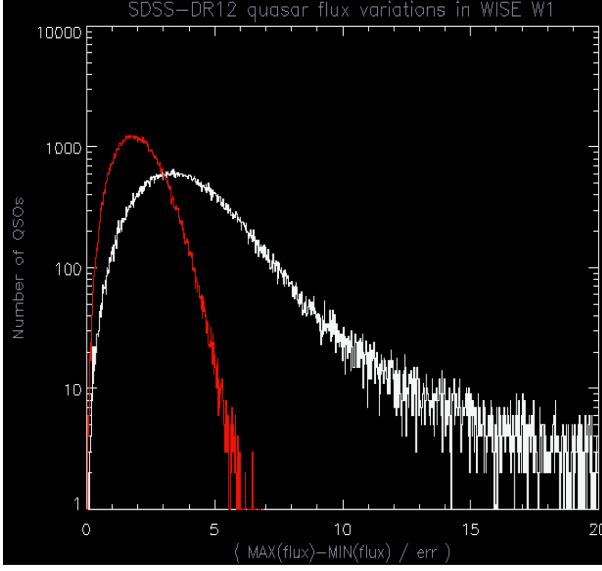


FIG. 2.— Here, “err” is the quadrature sum of the errors at the minimum and maximum fluxes. The red histogram is the expected distribution if these objects had no variability, and the errors were normally-distributed for each of the epochs. This shows that $\sim 6,000$ quasars are $> 10\sigma$ detections of variability in W1.

photometry at the locations of DECam-detected optical sources. This forced photometry is performed on time-resolved unWISE coadds, each of which represents a stack with depth of coverage ~ 12 exposures. A given sky location is observed by WISE for ~ 1 day once every six months, which means that our forced photometry light curves typically have four coadd epochs available. Coadd epochs of a given object are separated by a minimum of six months and a maximum of four years. Our coaddition removes the possibility of probing variability on $\lesssim 1$ day time scales, but it allows us to push ~ 1.4 magnitudes deeper than individual exposures while removing virtually all single-exposure artifacts (e.g. cosmic rays and satellites).

$\sim 30,000$ of the SDSS quasars with such W1/W2 lightcurves available are “IR-bright”, in the sense that they are above both the W1 and W2 single exposure thresholds and therefore detected at very high significance in our coadds. For this ensemble of objects, the typical variation in each quasar’s measured ($W_1 - W_2$) color is 0.06 magnitudes, which includes statistical and systematic errors expected to contribute variations at the few hundredths of a mag level. The typical measured single-band scatter is 0.07 magnitudes in each of W1 and W2. A full characterization of the typical mid-IR quasar variability will be presented separately (Ross et al., in preparation).

We undertook a search for extreme outliers relative to these trends. Specifically, we selected objects with the following characteristics.

- Monotonic variation in both W1 and W2.
- W1 versus W2 flux correlation coefficient > 0.9 .
- > 0.5 mag peak-to-peak variation in either W1 or W2.

This yielded a sample of 248 sources. 31 of these are assumed to be blazars due to the presence of FIRST ra-

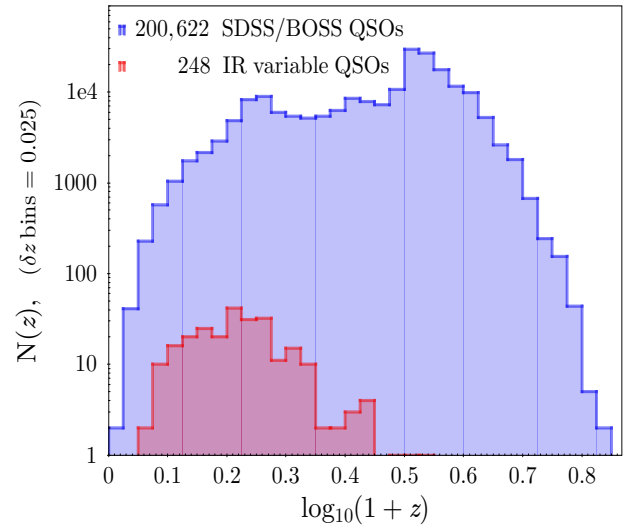


FIG. 3.— The the variations in ($W_1 - W_2$) color using $\sim 37,500$ data points from ~ 9000 bright quasars. Overplotted is a Gaussian distribution, centered at -3.8 mmag and with standard deviation of 0.06 mags (with a fit-by-eye :-).

dio counterparts. Another 22 are outside of the FIRST footprint, leaving 195 quasars in our IR-variable sample. We randomly selected five of these objects for follow-up spectroscopy with Palomar DBSP on the night of 30 January 2017. WISE J1052+1519, one of these five, faded by 0.75 (0.9) mags in W1 (W2), and thus became 0.15 mags bluer in ($W_1 - W_2$), making it a significant outlier in both single-band and IR color variability.

A link to the key properties of our sample can be found [here](#) and the catalogs are here: dr3_wise_lc_sample.fits.gz dr3_wise_lc_sample.fits.gz. The first catalog has 248 rows, which are the selected highly IR-variable sample of objects. The second catalog is the full 200 622 quasar sample quasars that have “good” WISE light curves available in DECaLS DR3. In each file, there are 3 extensions: ex = 0 – WISE light curve summary metrics; ex = 1 – DECaLS DR3 Tractor data for each object; ex = 2 – SDSS data for each object.

3. RESULTS: GENERAL POPULATION

Starting from the $\approx 200,000$ object parent quasar sample, and employing the selections as described above, we generate a catalog of 248 objects. Some general properties include:

- The redshift distribution of the IR-variable sample of objects being at generally lower redshift than the parent sample, but extending to relatively high- z - see Figure 3;
- 221 (89%) of the sample have falling IR lightcurves.
- The extremely IR variable QSOs generally have the same optical colors as the parent population, see Figures 6 and 7.

The $N(z)$ redshift distributions are shown in Figure 3 with the parent sample the blue histogram and the IR-variable sample the red histogram.

Lorem ipsum dolor sit amet, consectetur adipiscing elit. Aliquam porta sodales est, vel cursus risus porta

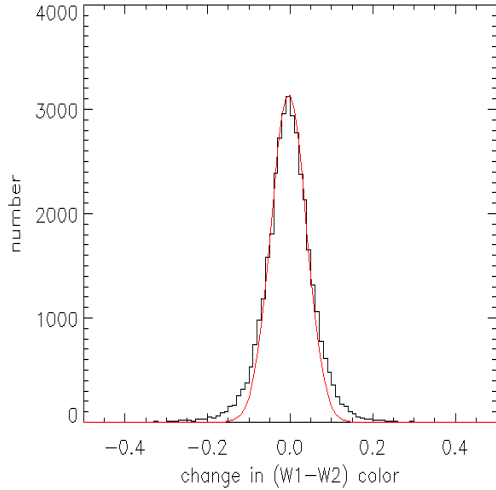


FIG. 4.— The variations in $(W_1 - W_2)$ color using $\sim 37,500$ data points from ~ 9000 bright quasars. Overplotted is a Gaussian distribution, centered at -3.8 mmag and with standard deviation of 0.06 mags (with a fit-by-eye ;-).

non. Vivamus vel pretium velit. Sed fringilla suscipit felis, nec iaculis lacus convallis ac. Fusce pellentesque condimentum dolor, quis vehicula tortor hendrerit sed. Class aptent taciti sociosqu ad litora torquent per conubia nostra, per inceptos himenaeos. Etiam interdum tristique diam eu blandit. Donec in lacinia libero.

3.1. Color Changes

Figure 4 shows the variations in the $(W_1 - W_2)$ color, which is pretty narrow. Overplotted is a Gaussian distribution, centered at -3.8 mmag and with standard deviation of 0.06 mags.

This histogram includes $\sim 37,500$ data points from ~ 9000 bright quasars, that is, brighter than single-exposure detection limit in both W_1 and W_2 . *NPR: It'd be very most awesome if we could show a $W_1W_2W_3$ RGB image of a quasar changing color!!!*

Figure 5 has the same data as Fig 4, now in a scatterplot of $\Delta(W_1)$ versus $\Delta(W_2)$. There is clearly some variation, and it is well-correlated between W_1 and W_2 . The red line is $x = y$. (I would guess this is real variation, but I'm still a little bit scared that you could have e.g. correlated background level issues in the coadds that imprint onto the fluxes.)

Etiam mollis viverra nisi eget aliquet. Aliquam erat volutpat. Vivamus tristique, nisl eu malesuada semper, libero tortor convallis elit, a scelerisque orci nisi lacinia turpis. In lacinia ultrices volutpat. Proin ultrices luctus tellus, in placerat eros tincidunt id. Ut varius iaculis quam in consequat. Nulla nec orci est, sit amet pellentesque nisl. Mauris non cursus lectus. Praesent placerat leo vel erat gravida lacinia. Donec vehicula consectetur lectus vitae luctus. Praesent nisl justo, laoreet elementum facilisis vel, tristique ac enim. Etiam vel quam ut quam eleifend tincidunt. Suspendisse sit amet eros vel elit ullamcorper laoreet. Etiam venenatis sodales turpis, nec lacinia ligula hendrerit nec. Nam eu vulputate purus. Quisque facilisis congue metus, sed imperdiet lorem rhoncus sit amet.

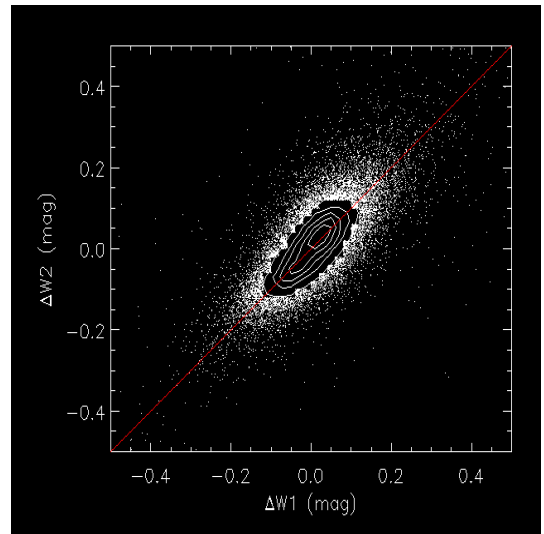


FIG. 5.— The variations in $(W_1 - W_2)$ color using $\sim 37,500$ data points from ~ 9000 bright quasars. Overplotted is a Gaussian distribution, centered at -3.8 mmag and with standard deviation of 0.06 mags.

3.2. Changes in color: One IR Variable population or two?

Turpis tincidunt quam consectetur non suscipit telus placerat. Etiam sit amet justo condimentum sem scelerisque pharetra. Nullam sit amet neque eget quam tempor consectetur vel vitae massa. Nunc porttitor, quam in tempor pharetra, leo libero eleifend mi, ac ornare nibh eros vel purus. Pellentesque lobortis enim metus.

4. RESULTS: INDIVIDUAL OBJECTS

4.1. SDSS J110057.71-005304.5

Figures ?? presents the IR NEOWISER light curve for J110057, and 9 the IR finding charts.

SDSS J110057.71-005304.5, hereafter J110057, was discovered by the Sloan Digital Sky Survey in 2000. J110057 was imaged in Run 756 (which makes up Stripe 10), and satisfied a number of spectroscopic targettings flags⁵ making it a quasar target. A spectrum was obtain on MJD 51908, on Plate 277, Fiber 212, and the spectrum of a $z = 0.378 \pm 0.00003$ was

In the DECaLS, the DECaLS brick containing J110057.71-005304.5. There are 8, 3 and 9 exposures in the g -, r - and z -band respectively. $56707.146 \leq g_{\text{MJD}} \leq 56727.201$; $56367.091 \leq r_{\text{MJD}} \leq 56367.230$; $56383.159 \leq z_{\text{MJD}} \leq 57398.350$.

As can be seen, the g - and r -band observations have fairly limited time spans, and are separated by roughly a year. The z -band observations span almost 3 years. The DESI imaging brick name is 1651m010.

Second epoch spectrum is from BOSS and has a dramatic downturn at $\lesssim 4300\text{\AA}$.

A third epoch spectrum was obtained from the Palomar 5m telescope using the DBSP instrument. Two exposures of 600s+300s were taken in good conditions. Feature to note include: the continuum straddling MgII being blue in the 2017 spectrum, as it was for the SDSS

⁵ SERENDIP_BLUE, ROSAT_D, ROSAT_C, ROSAT_B, QSO_SKIRT, ROSAT_A, see ? and Richards et al. (2002) for flag descriptions.

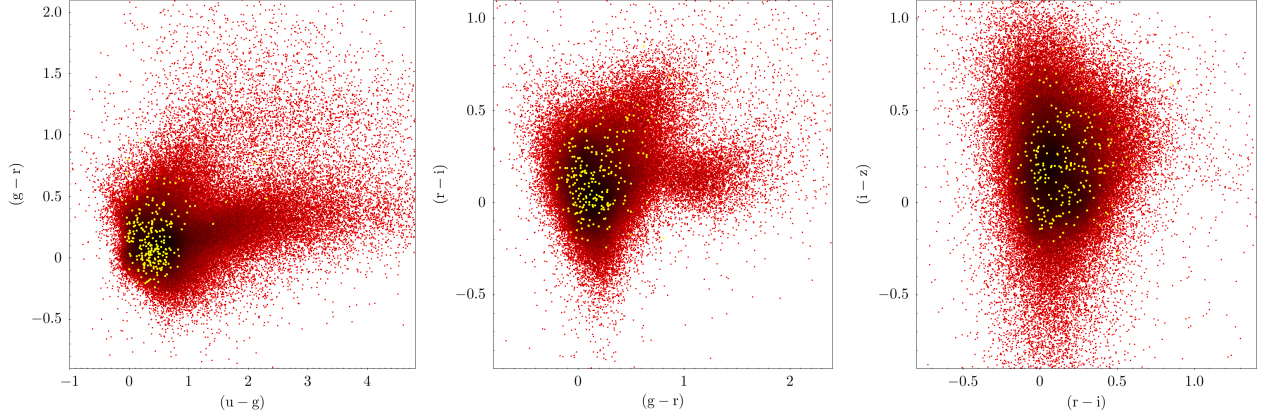


FIG. 6.— The $ugriz$ color-color plots for the full 200k super-sample (red points) and the 248 extreme IR variables (yellow dots).

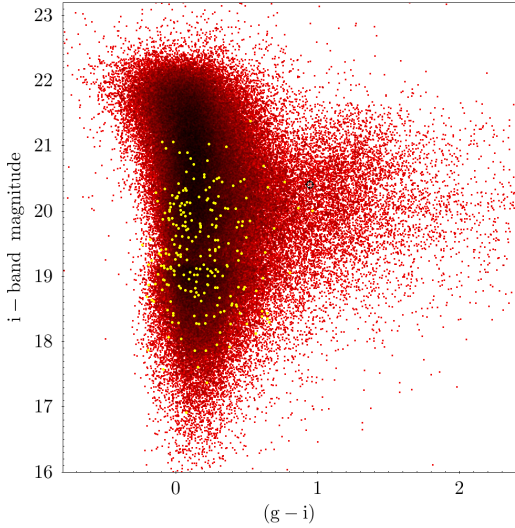


FIG. 7.— The color-mag and grz color-color plots for the full 200k super-sample (red points) and the 248 extreme IR variables (yellow).

spectrum in 2000, as opposed to red, as it was for the BOSS spectrum in 2010.

Lorem ipsum dolor sit amet, consectetur adipiscing elit. Aliquam porta sodales est, vel cursus risus porta non. Vivamus vel pretium velit. Sed fringilla suscipit felis, nec iaculis lacus convallis ac. Fusce pellentesque

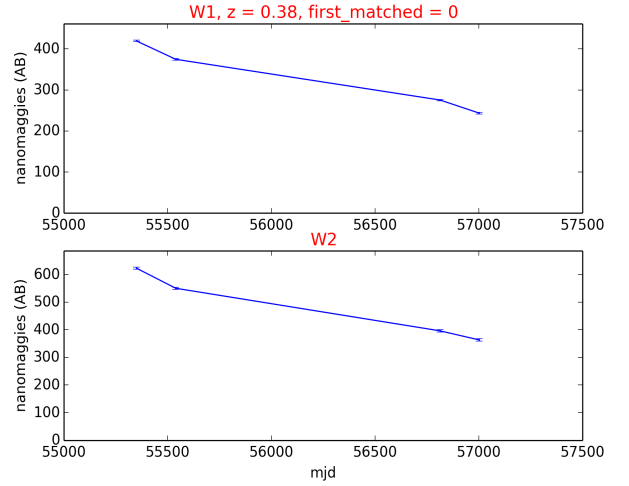


FIG. 8.— WISE infrared light-curve for J110057.

condimentum dolor, quis vehicula tortor hendrerit sed. Class aptent taciti sociosqu ad litora torquent per conubia nostra, per inceptos himenaeos. Etiam interdum tristique diam eu blandit. Donec in lacinia libero.

Sed elit massa, eleifend non sodales a, commodo ut felis. Sed id pretium felis. Vestibulum et turpis vitae quam aliquam convallis. Sed id ligula eu nulla ultrices tempus. Phasellus mattis erat quis metus dignissim malesuada. Nulla tincidunt quam volutpat nibh facilisis euismod. Cras vel auctor neque. Nam quis diam risus.

Nunc semper quam et leo interdum vulputate eu quis magna. Sed nec arcu at orci egestas convallis. Aenean quam velit, aliquam vitae viverra in, elementum vel elit. Nunc suscipit aliquet sapien a suscipit. Cras nulla ipsum, posuere eu fringilla sit amet, dapibus ultricies nulla. Nullam eu augue id purus mollis dignissim sed et libero. Phasellus eget justo sed neque pellentesque egestas nec id arcu. Donec facilisis pulvinar sapien et fringilla. Suspendisse vestibulum rhoncus sapien id laoreet. Morbi et orci vitae tortor imperdiet imperdiet. In hac habitasse platea dictumst. Vivamus vel neque id mi ultrices tristique. Integer quam libero, ornare vel gravida in, feugiat a ante. Nam dapibus, tellus vitae pellentesque cursus, duis nisl egestas augue, non fermentum nisl est nec nisi. Vestibulum nec mi justo, eget dapibus velit.

5. DISCUSSION

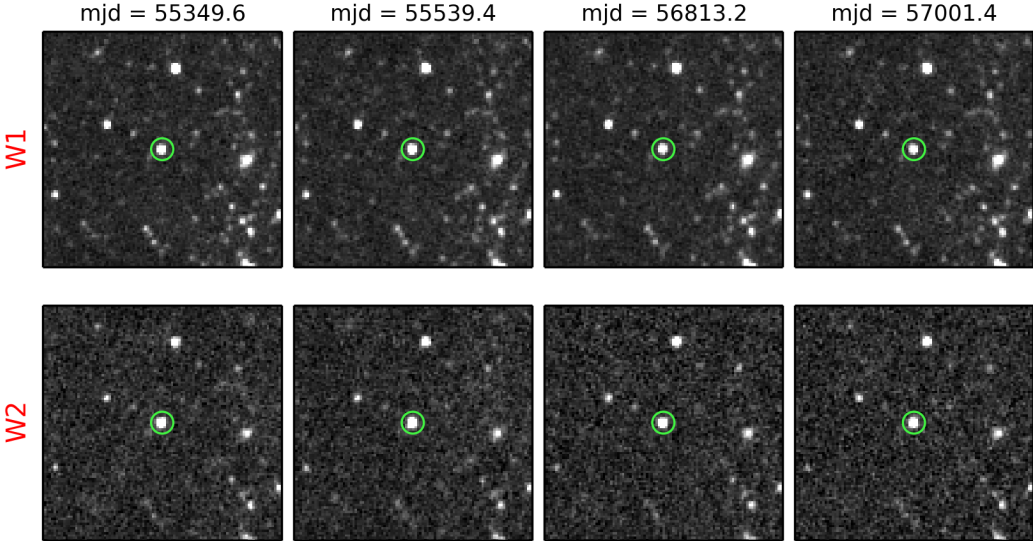


FIG. 9.— WISE thumbnail images for J110057.

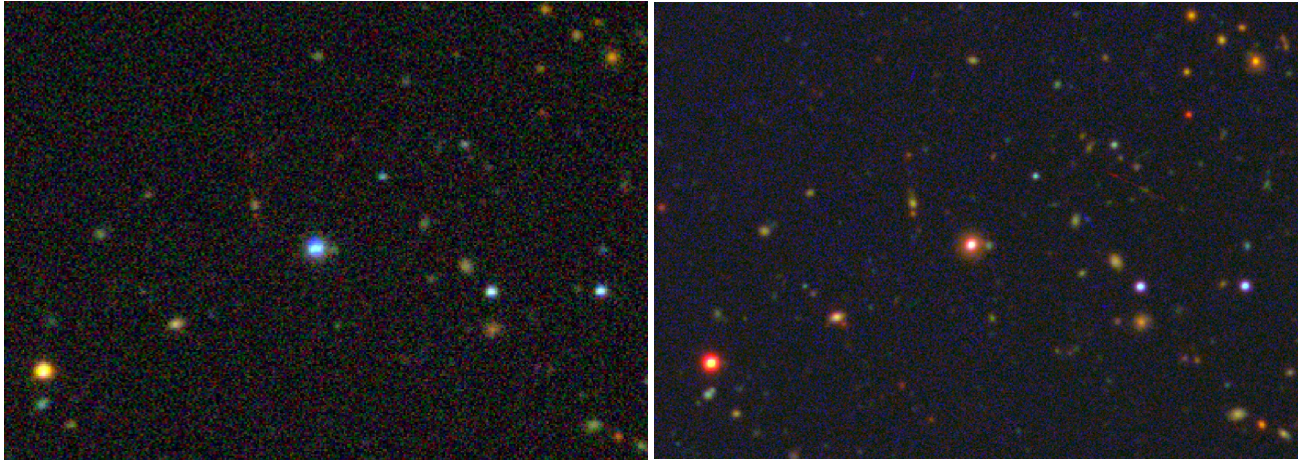


FIG. 10.— The SDSS (*left* and DECaLS (*right*) image of SDSS J110057.71-005304.5 (center).

Sed elit massa, eleifend non sodales a, commodo ut felis. Sed id pretium felis. Vestibulum et turpis vitae quam aliquam convallis. Sed id ligula eu nulla ultrices tempus. Phasellus mattis erat quis metus dignissim malesuada. Nulla tincidunt quam volutpat nibh facilisis euismod. Cras vel auctor neque. Nam quis diam risus.

Nunc semper quam et leo interdum vulputate eu quis magna. Sed nec arcu at orci egestas convallis. Aenean quam velit, aliquam vitae viverra in, elementum vel elit. Nunc suscipit aliquet sapien a suscipit. Cras nulla ipsum, posuere eu fringilla sit amet, dapibus ultricies nulla. Nullam eu augue id purus mollis dignissim sed et libero. Phasellus eget justo sed neque pellentesque egestas nec id arcu. Donec facilisis pulvinar sapien et fringilla. Suspendisse vestibulum rhoncus sapien id laoreet. Morbi et orci vitae tortor imperdiet imperdiet. In hac habitasse platea dictumst. Vivamus vel neque id mi ultrices tristique. Integer quam libero, ornare vel gravida in, feugiat a ante. Nam dapibus, tellus vitae pellentesque cursus, duis nisl egestas augue, non fermentum nisl est nec nisi. Vestibulum nec mi justo, eget dapibus velit.

6. DISCUSSION AND CONCLUSIONS

Sed non felis iaculis dui iaculis mattis facilisis ullamcorper ipsum. Donec erat nunc, consectetur et ornare in, egestas vitae mauris. Praesent suscipit rutrum purus, in interdum tellus euismod sit amet. Nulla facilisi. Etiam nisl ligula, vehicula at fringilla et, sagittis eu odio.

Our conclusions are thus:

- Hendrerit pretium commodo. Cras dapibus fringilla dolor a ultrices. Morbi bibendum neque in magna pellentesque rhoncus. Sed vitae lorem lacus.
- Pellentesque nec justo et dolor scelerisque fermentum. Vivamus augue libero, fermentum id tristique at, suscipit ultricies turpi.
- Cras in laoreet mauris. Vivamus nec nulla a dui commodo adipiscing. Proin vulputate lectus nec arcu iaculis sit amet auctor ligula ultricies. Phasellus condimentum gravida tincidunt. Phasellus et mauris ac nibh vestibulum vehicula.

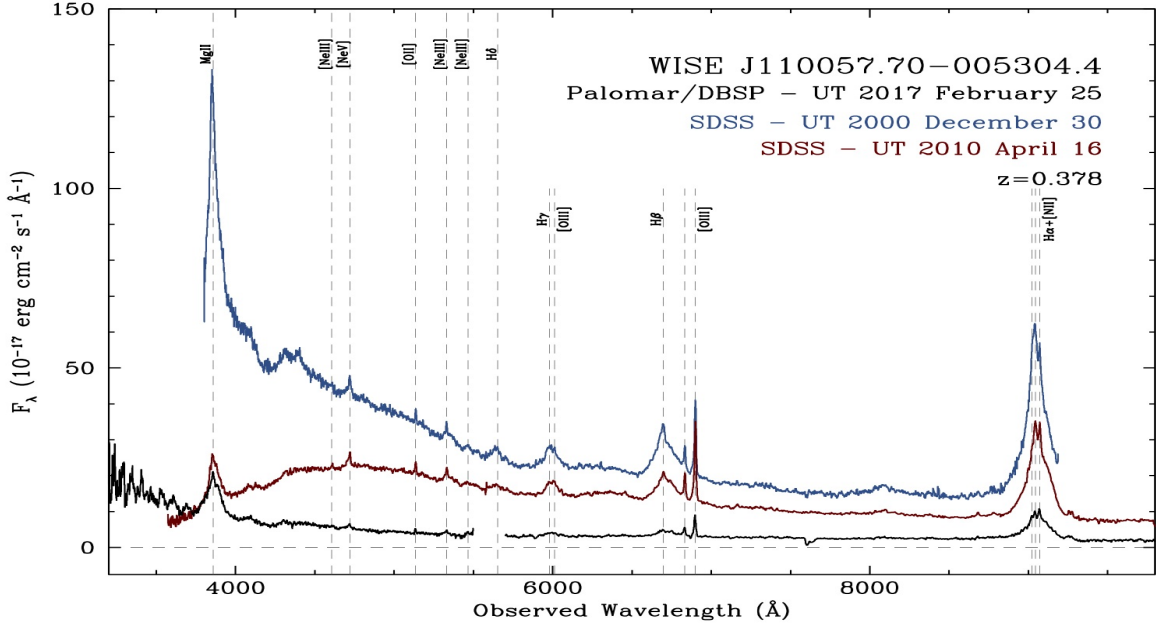
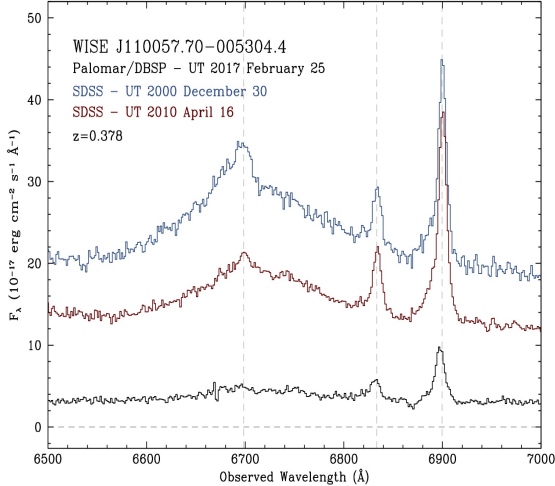


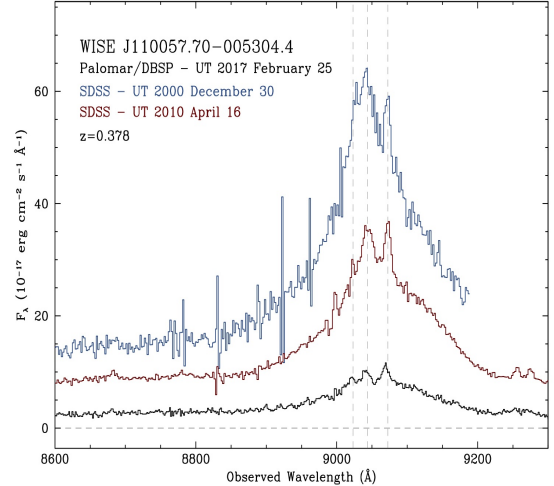
FIG. 11.—

FIG. 12.— SDSS J110057.71-005304.5 H β zoom-in.

Morbi et augue id purus gravida sagittis quis in sem. Phasellus quis risus bibendum eros luctus auctor. Proin non tempus velit. Etiam laoreet, enim nec scelerisque dictum, tortor massa tempor enim, id pretium justo quam ac lectus. Maecenas diam nibh, interdum at lobortis sit amet, dignissim et quam. Sed tincidunt faucibus risus, congue tempus nisl consectetur eget. Suspendisse venenatis turpis ut risus aliquam interdum. In at velit sed ligula dictum dignissim ut et dui. Curabitur ac scelerisque purus.

7. ACKNOWLEDGMENTS

We thank the IPAC team for the Explanatory Supplement to the WISE All-Sky and AllWISE Data Release Products resource. NEOWISE and NEOWISE-R makes

FIG. 13.— SDSS J110057.71-005304.5 H α zoom-in.

use of data from WISE, which is a joint project of the University of California, Los Angeles, and the Jet Propulsion Laboratory/California Institute of Technology, and NEOWISE, which is a project of the Jet Propulsion Laboratory/California Institute of Technology. WISE and NEOWISE are funded by the National Aeronautics and Space Administration.

This research made use of the NASA Astrophysics Data System. This research also made use of the astropy.org codebase (proper citation). The data and code used herein will become publicly available at upon publication of the paper.

N.P.R. acknowledges support from the STFC and the Ernest Rutherford Fellowship scheme.

Funding for the SDSS and SDSS-II has been provided by the Alfred P. Sloan Foundation, the Participating Institutions, the National Science Foundation, the US Department of Energy, the National Aeronautics and Space Administration, the Japanese Monbukagakusho, the Max Planck Society, and the Higher Education Funding Council for England. The SDSS web site is <http://www.sdss.org>.

Funding for SDSS-III has been provided by the Alfred P. Sloan Foundation, the Participating Institutions, the National Science Foundation, and the U.S. Department of Energy. The SDSS-III web site is <http://www.sdss3.org/>. SDSS-III is managed by the Astrophysical Research Consortium for the Participating Institutions of the SDSS-III Collaboration including the University of Arizona, the Brazilian Participation Group, Brookhaven National Laboratory, University of Cambridge, University of Florida, the French Participation Group, the German Participation Group, the Instituto de Astrofisica de Canarias, the Michigan State/Notre Dame/JINA Participation Group, Johns Hopkins University, Lawrence Berkeley National Laboratory, Max Planck Institute for Astrophysics, New Mexico State University, New York University, Ohio State University, Pennsylvania State University, University of Portsmouth, Princeton University, the Spanish Participation Group, University of Tokyo, University of Utah, Vanderbilt University, University of Virginia, University of Washington, and Yale University.

Facilities: SDSS, BOSS, WISE, CTIO Blanco+DECam

APPENDIX
TECHNICAL DETAILS

All good papers have to have an Appendix.

SDSS Info	Description	Example
SDSSJ	SDSS object name	000920.76+033021.7
RA	SDSS object R.A. (J2000)	002.33654086687
DEC	SDSS object Decl.(J2000)	+003.50603303134
Z	SDSS (pipeline) redshift	0.432505905628
MJD	Modified Julian Date	55806
FIBER	Fiber number	0196
PLATE	Plate number	4297
U_FLUX	u-band flux	10.1695
G_FLUX	g-band flux	13.8142
R_FLUX	r-band flux	14.1181
I_FLUX	i-band flux	16.7872
Z_FLUX	z-band flux	21.7649
DR	Data Release number	12
FIRST_MATCHED	Matched in FIRST radio survey?	0
WISE LC Metrics	Description	Example
MEAN_SNR_W1	Mean Signal-to-noise, W1	38.8656
MEAN_SNR_W2	Mean Signal-to-noise, W2	22.8657
PEARSON_R	Pearson correlation coefficient	0.999489
N_EPOCH	number of WISE epochs	4
NBAD_W1	Quality flag for epochs??	0
NBAD_W2	Quality flag for epochs??	0
MONO_W1	a	1
MONO_W2	b	1
BEST_FLUX_W1	c	72.078
BEST_FLUX_W2	d	94.7315
CHI2_W1	e	170.705
CHI2_W2	f	88.7313
RCHI2_W1	g	56.9016
RCHI2_W2	h	29.5771
FLUX_MIN_W1	i	56.8723
FLUX_MAX_W1	j	86.1033
FLUX_MIN_W2	k	69.1232
FLUX_MAX_W2	l	114.478
MAG_RANGE_W1	m	0.450297
MAG_RANGE_W2	n	0.547747
GOOD_EPOCH_MASK o	[1 1 1 1 0]	
RISING_W1	p	0
FALLING_W1	q	1
RISING_W2	r	0
FALLING_W2	s	1
COADD_ID	t	0030p030
X_COADD	u	1923.45
Y_COADD	v	1648.51
Name	Description	Example
BRICKID	Brick ID [1,662174]	
BRICKNAME	Name of brick, near RA=112.6, Dec=+22.2	eg "1126p222"
OBJID	Catalog object number within this brick;	
BRICK_PRIMARY	a unique identifier hash is BRICKID,OBJID;	
BLOB	True if the object is within the brick boundary	
NINBLOB	Blend family;	contiguously numbered from 0
TYCHO2INBLOB	Number of sources in this BLOB	
TYPE	Is there a Tycho-2 (very bright) star in this blob?	
RA	Morphological model	
RA_IVAR	Right ascension at epoch J2000	
DEC	Inverse variance of RA	
DEC_IVAR	Declination at epoch J2000	
BX	Inverse variance of DEC (no cos term!)	
BY	X position of coordinates in brick image stack	
	Y position of coordinates in brick image stack	

SPECTROPHOTOMETRY FOR CHANGING LOOK QSO 3836/55302-258

All really good papers have more than one Appendix.

REFERENCES

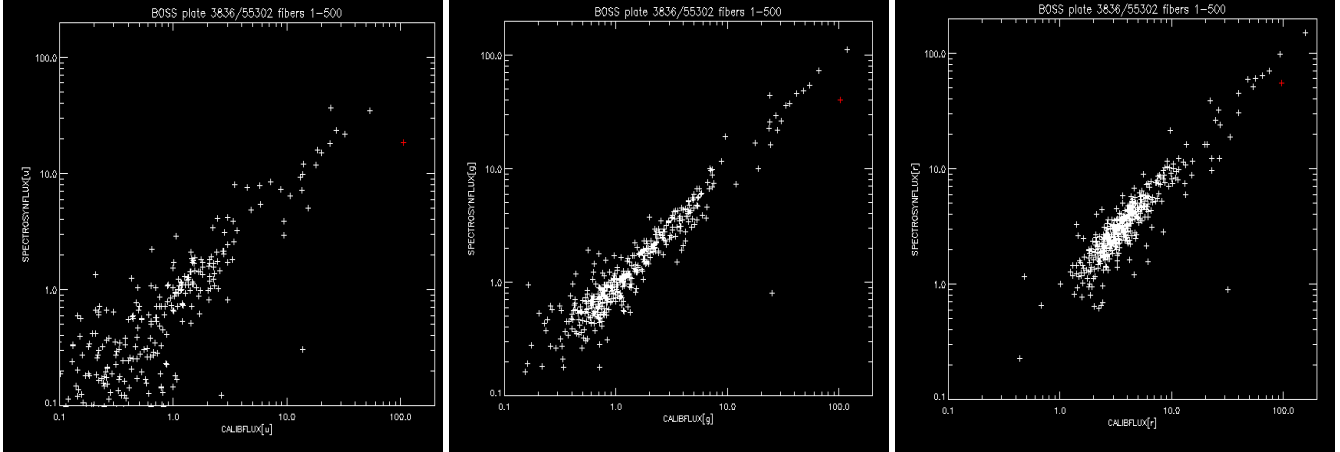


FIG. 14.— The spectrophotometry checks for Changing Look QSO SDSS J110057. From left to right, the u , g and r bands. Along the x -axis is a measurement of the “calibration flux” photometric value which is an estimate of the flux within a 2 arcsecond aperture, and which is the PSF flux value for point objects (stars). On the y -axis is the spectrophotometric flux values. For the SDSS u , g and r -bands from left to right. J110057 is the red point, and is clearly off the general trends for the 500 objects on this half-plate for one the BOSS spectrographs, but is close to the trend in r -band strongly suggesting the variations observed in the BOSS spectra are real.

- Assef R. J., et al., 2013, ApJ, 772, 26
 Banerji M., McMahon R. G., Hewett P. C., Gonzalez-Solares E., Koposov S. E., 2013, MNRAS, 429, L55
 Becker R. H., White R. L., Helfand D. J., 1995, ApJ, 450, 559
 Bower R. G., Schaye J., Frenk C. S., Theuns T., Schaller M., Crain R. A., McAlpine S., 2017, MNRAS, 465, 32
 Dawson K., et al., 2013, AJ, 145, 10
 Donley J. L., et al., 2012, ApJ, 748, 142
 Draine B. T., 2003, ARA&A, 41, 241
 Eisenstein D. J., Weinberg D. H., et al., 2011, AJ, 142, 72
 Elitzur M., 2014, MNRAS, 438, 3340
 Fukugita M., Ichikawa T., Gunn J. E., Doi M., Shimasaku K., Schneider D. P., 1996, AJ, 111, 1748
 Gunn J. E., et al., 1998, AJ, 116, 3040
 Gunn J. E., et al., 2006, AJ, 131, 2332
 Hogg D. W., Finkbeiner D. P., Schlegel D. J., Gunn J. E., 2001, AJ, 122, 2129
 Ivezic Z., et al., 2004, Astronomische Nachrichten, 325, 583
 Kozłowski S., et al., 2010, ApJ, 716, 530
 Kozłowski S., Kochanek C. S., Ashby M. L. N., Assef R. J., Brodwin M., Eisenhardt P. R., Jannuzi B. T., Stern D., 2016, ApJ, 817, 119
 Lacy M., et al., 2004, ApJS, 154, 166
 Lang D., 2014, AJ, 147, 108
 Lang D., Hogg D. W., Schlegel D. J., 2016, AJ, 151, 36
 Lupton R., Gunn J. E., Ivezic Z., Knapp G. R., Kent S., 2001, in F. R. Harnden Jr., F. A. Primini, & H. E. Payne ed., Astronomical Data Analysis Software and Systems X Vol. 238 of Astronomical Society of the Pacific Conference Series, The SDSS Imaging Pipelines. p. 269
 Mainzer A., et al., 2014, ApJ, 792, 30

- Martínez-Sansigre A., Rawlings S., Lacy M., Fadda D., Jarvis M. J., Marleau F. R., Simpson C., Willott C. J., 2006, MNRAS, 370, 1479
 McAlpine S., Bower R. G., Harrison C. M., Crain R. A., Schaller M., Schaye J., Theuns T., 2017, ArXiv e-prints
 Meisner A. M., Lang D., Schlegel D. J., 2016, ArXiv e-prints
 Netzer H., 2015, ARA&A, 53, 365
 Oke J. B., Gunn J. E., 1983, ApJ, 266, 713
 Padmanabhan N., et al., 2008, ApJ, 674, 1217
 Pâris I., Petitjean P., Ross N. P., et al., 2017, Astron. & Astrophys., 597, A79
 Pier J. R., Munn J. A., Hindsley R. B., Hennessy G. S., Kent S. M., Lupton R. H., Ivezic Z., 2003, AJ, 125, 1559
 Pillepich A., et al., 2017, ArXiv e-prints
 Richards G. T., et al., 2002, AJ, 123, 2945
 Richards G. T., et al., 2009, AJ, 137, 3884
 Richards G. T., et al., 2015, ApJS, 219, 39
 Rosas-Guevara Y., Bower R. G., Schaye J., McAlpine S., Dalla Vecchia C., Frenk C. S., Schaller M., Theuns T., 2016, MNRAS, 462, 190
 Ross N. P., et al., 2012, ApJS, 199, 3
 Schneider D. P., et al., 2010, AJ, 139, 2360
 SDSS Collaboration Albareti F. D., Allende Prieto C., Almeida A., Anders F., Anderson S., Andrews B. H., Aragon-Salamanca A., Argudo-Fernandez M., Armengaud E., et al. 2016, ArXiv e-prints
 Shen Y., et al., 2011, ApJS, 194, 45
 Smith J. A., et al., 2002, AJ, 123, 2121
 Stern D., et al., 2005, ApJ, 631, 163
 Stern D., et al., 2012, ApJ, 753, 30
 Stoughton C., et al., 2002, AJ, 123, 485
 Timlin J. D., et al., 2016, ApJS, 225, 1
 Tucker D. L., et al., 2006, Astronomische Nachrichten, 327, 821
 Wright E. L., et al., 2010, AJ, 140, 1868
 York D. G., et al., 2000, AJ, 120, 1579